J Mater Sci (2007) 42:10164–10172
DOI 10.1007/s10853-007-2102-z

Voltammetric and chronoamperometric studies of silver electrodeposition from a bath containing HEDTA

G. M. de Oliveira · M. R. Silva · Ivani Aparecida Carlos

Received: 21 June 2007 / Accepted: 13 August 2007 / Published online: 25 September 2007

Abstract The electrodeposition of silver on platinum from ammonium-buffered solutions containing HEDTA (N-(2-hydroxyethyl)ethylenediaminetriacetic acid) at various concentrations was investigated. Potentiometric titration and voltammetric studies indicated that in the presence of 2.0×10^{-1} M HEDTA, the deposited silver was reduced from a mixture of $[AgHEDTA]^{2-}$ and $[Ag(NH_3)_2]^+$ complexes, whereas at 2.0×10^{-2} M and 2.0×10^{-3} M HEDTA in the electrolyte, the silver was reduced from the $[Ag(NH_3)_2]^+$ complexes alone. Hydrodynamic studies showed variation in the diffusion coefficient for the electroactive species in solution, depending on the HEDTA concentration. Chronoamperometric study in a solution containing 2.0×10^{-1} M HEDTA at low overpotential (0.000 V to –0.050 V) showed a transition from progressive to instantaneous nucleation in a single current transient, whereas, at –0.200 V only 3*D*-progressive nucleation controlled by mass transport was observed. Scanning electron microscope images showed that the silver films produced in silver baths with HEDTA were uniform, without cracks, and fine-grained, regardless of its concentration, while in the absence of HEDTA the morphology was rough and dendritic. X-ray diffraction analysis of the films obtained at various HEDTA concentrations revealed polycrystalline silver, similar to film obtained in cyanide and EDTA/ammonia baths.

G. M. de Oliveira · M. R. Silva · I. A. Carlos (✉)
Departamento de Química, Universidade Federal de São Carlos, CP 676, Sao Carlos, SP 13565-905, Brazil
e-mail: diac@power.ufscar.br

Introduction

An extensive search has been made in the electroplating industry for novel electrolytes for silver electrodeposition as alternative to cyanide solutions [1–16]. For this purpose, several additives are employed in the plating bath for their beneficial effect on film morphology. In general, these additives are organic substances, which may act as smoothing, brightening, complexing agents, etc.

Silver electrodeposition on a platinum substrate from silver nitrate solutions, without any additives in the plating bath, results in poor films, which are formed by clusters of crystallites and dendrites dispersed on the Pt substrate [17]. In addition, it has been observed that silver film deposited on platinum from ammonium-buffered solutions has a similar morphology, although the substrate is covered better. On the other hand, the presence of the EDTA (ethylenediaminetetraacetic acid) in the plating bath leads to films of high quality [15].

In this study, silver electrodeposition on platinum was investigated in ammonium-buffered solutions with various concentrations of HEDTA (N-(2-hydroxyethyl)ethylenediaminetriacetic acid), an aminopolycarboxylate ligand similar to EDTA. Although the additives HEDTA and EDTA are similar, they can affect the silver electrodeposition process differently, since different charged species can be formed at a specific pH, leading to silver films with distinct morphologies. The results described here illustrate how the HEDTA influenced the deposition kinetics, the mechanism by which the crystals nucleate and grow and the morphology and the structure of the silver electrodeposits.

Experimental details

All chemicals were analytical grade. Double-distilled water was used throughout. Each electrochemical experiment was performed in a freshly prepared solution, containing 1.0×10^{-1} M $AgNO_3$ + x HEDTA + 5.0×10^{-1} M NH_3 + 1.0×10^{-1} M NH_4NO_3 (pH = 10.5), where x may be 0 M; 2.0×10^{-3} M; 2.0×10^{-2} M; and 2.0×10^{-1} M.

Potentiometric measurements were performed with a Micronal B474 pH-meter. A silver wire of 2 cm and calomel (Hg/Hg_2Cl_2, 1.0 M KCl) were used as indicator and reference electrodes, respectively.

Voltammetric and chronoamperometric curves were recorded with an EG&G PAR electrochemical system consisting of a Potentiostat/Galvanostat, model 173 and the signal were recorded by x-y-t ECB RB400 recorder. Hydrodynamic measurements were carried out with a rotating disk electrode system, PAR model 366. Deposition charge density was measured with an EG&G PAR Coulometer 179. All experiments were carried out at room temperature (25 °C). A platinum disk (0.196 cm^2), a Pt plate, and an appropriate Lugging capillary containing Hg/HgO, 1.0 M NaOH, were employed as working, auxiliary, and reference electrodes, respectively. Immediately prior to the electrochemical measurements, the working electrode was rinsed with a mixture of concentrated sulfuric and nitric acids. All values of current density shown in the voltammetric and chronoamperometric curves were calculated with respect to the initial platinum electrode area. In this work we studied the influence of HEDTA on the deposition process and in the morphology and structure of silver deposit, then, the platinum substrate was only employed as work electrode due to its noble character.

Scanning Electron Microscopy (SEM) photographs were taken with a Leica Stereoscan 440 [15, 18–25].

X-ray diffraction (XRD) patterns were produced with Cu Kα radiation (1.5406 Å), using a Rigaku Rotaflex RU200B X-ray goniometer, in 2θ scanning mode (fixed $\omega = 2°$) [15, 19, 20, 24–26].

SEM and XRD analyses were carried out on silver films deposited by chronoamperometry at –0.200 V (referred to the Hg/HgO, 1.0 M NaOH electrode) with 2.0 C cm^{-2}.

Results and discussion

Potentiometric titration study

In order to establish the species of complex formed in the electrolytic solutions used in this study of silver deposition, a series of potentiometric titrations were performed (Fig. 1). The potential values were referred to the Hg/Hg_2Cl_2, 1.0 M KCl electrode, which was only used for potentiometric titrations. Table 1 shows the composition of the solutions used in the titrations shown in Fig. 1 and the respective ratios of $[HEDTA]/[Ag^+]$ and $[NH_3]/[Ag^+]$ at the end point.

When $AgNO_3$ was titrated with HEDTA (Y^{3-}), (Fig. 1(□ □ □)), a well-defined end point was seen at a ratio of 1.17:1.00 $[HEDTA]/[Ag^+]$, indicating the formation of the complex ion $[AgHEDTA]^{2-}$. However, the titration with ammonium-buffered solution (Fig. 1(■ ■ ■)) showed an end point at 1.96:1.00 ratio of $[NH_3]/[Ag^+]$, which corresponds to the ion complex $[Ag(NH_3)_2]^+$. It is important to observe that the potentials of the electrode at the end of the two titrations were very close, since the complex ions $[AgHEDTA]^{2-}$ and $[Ag(NH_3)_2]^+$ have similar stability constants (β), i.e., $10^{6.7}$ and $10^{7.24}$, respectively [27]. This result showed that $[AgHEDTA]^{2-}$ and $[Ag(NH_3)_2]^+$ were the main complex species formed in solution containing HEDTA and ammonia, respectively.

With the purpose of finding out whether solutions containing NH_3 and HEDTA, a mixed complex could be formed, for example $[Ag(NH_3)(HEDTA)]^{2-}$, or a mixture of complex ions, various titrations with differing ratios of $[NH_3]/[HEDTA]$ were performed. Also, the effect of ammonium nitrate on the titration process was verified.

During the titration, for any mixed complex, the end point should be given by the limiting-ligand reactant and silver ion concentrations for the various ratios of $[NH_3]/[HEDTA]$ in the solution. The titration curves for solutions containing NH_3 and HEDTA showed one end point each (Fig. 1: S_3, S_4, S_5, and S_6). In this case, it was found that on increasing or decreasing the ratio of $[NH_3]/[HEDTA]$ from 2.5 to 5.0 or 1.3, neither $[HEDTA]/[Ag^+]$ nor $[NH_3]/[Ag^+]$

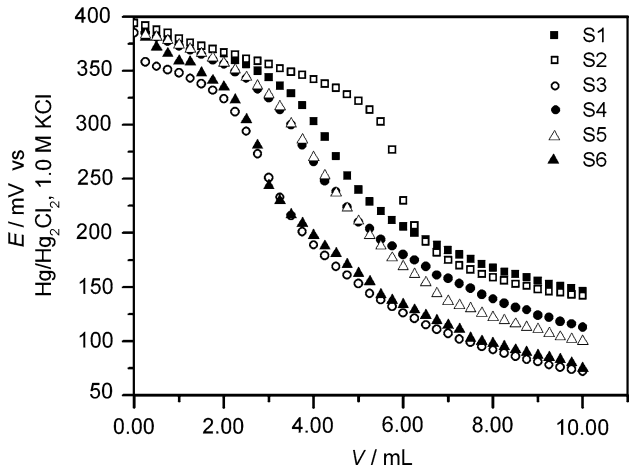

Fig. 1 Potentiometric titration curve of 50 mL of 2.00×10^{-2} M $AgNO_3$ with solutions of NH_3, HEDTA, or NH_3 + HEDTA with different ratios of NH_3 and HEDTA. The compositions of these solutions are given in Table 1. Potential values were referred to the Hg/Hg_2Cl_2, 1.0 M KCl electrode

Table 1 Ratios of [HEDTA]/[Ag^+] and [NH_3]/[Ag^+] at the end point in the potentiometric titration of 50 mL of 2.00×10^{-2} M $AgNO_3$

	Solution in the burette	[NH_3]/[Ag^+]	[HEDTA]/[Ag^+]	*EP*
S1	4.39×10^{-1} M NH_3 + 8.76 10^{-2} M NH_4NO_3	1.96		
S2	2.0×10^{-1} M HEDTA		1.17	
S3	4.39×10^{-1} M NH_3 + 8.76 10^{-2} M NH_4NO_3 + 1.752×10^{-1} M HEDTA	1.21	0.484	1.09
S4	4.39×10^{-1} M NH_3 + 8.76 10^{-2} M NH_4NO_3 + 8.76 10^{-2} M HEDTA	1.44	0.287	1.00
S5	2.28×10^{-1} M NH_3 + 8.76×10^{-2} M NH_4NO_3 + 1.752×10^{-1} M HEDTA	0.910	0.699	1.15
S6	4.39×10^{-1} M NH_3 + 1.752×10^{-1} M HEDTA	1.21	0.481	1.08

remained similar at the end point. These results indicated that probably mixed complex were not formed. Actually, it is probable that formation of a mixture of two complexes did occur, viz., $[AgHEDTA]^{2-}$ and $[Ag(NH_3)_2]^+$, since these complexes have similar stability constants.

This hypothesis was supported by the fact that at the end point in the titration the following relation should apply:

$$EP = \left([NH_3]/2 + [HEDTA] \right) / [Ag^+] = 1 \quad (1)$$

where [NH_3], [HEDTA], and [Ag^+] are the total concentrations of the species at the end point (*EP*). Table 1 shows that *EP* was close to 1 for all the titrations containing NH_3 and HEDTA, indicating that in these solutions, mixtures of complexes $[AgHEDTA]^{2-}$ and $[Ag(NH_3)_2]^+$ were formed.

Moreover, it was shown that NH_4NO_3 did not affect the titration curve, showing that it was not necessary to consider its concentration in the calculation of the end point.

Electrochemical study

Voltammetric study

Figure 2(a) shows voltammetric curves for silver electrodeposition on a platinum electrode from solutions of various compositions, containing $AgNO_3$, HEDTA, NH_3, and NH_4NO_3. It was found that changing the [NH_3]/[NH_4^+] ratio in solution (Fig. 2, solid (——) and dashed (- - -) curves) did not alter the silver deposition potential, indicating that NH_4^+ did not affect the silver deposition potential. However, the current density was changed, probably due to NH_4^+ adsorption at the surface of the platinum electrode. Moreover, the voltammetric curves indicated that while the silver (I) ions were reduced from $[Ag(NH_3)_2]^+$ (Fig. 2, solid (——) curve) and from $Ag(HEDTA)^{2-}$ (Fig. 2, dotted (•••) curve) at approximately the same potential, the rate of silver reduction from $[Ag(HEDTA)]^{2-}$ was appreciably lower than from $[Ag(NH_3)_2]^+$, i. e., the current density for $[Ag(HEDTA)]^{2-}$ reduction in the potential region from 0.00 V down to –0.70 V was half that for $[Ag(NH_3)_2]^+$. This result can been explained by the fact that $[Ag(HEDTA)]^{2-}$ has a lower diffusion coefficient than $[Ag(NH_3)_2]^+$ and, in this potential region the kinetics is controlled by mass transport. When NH_3 and HEDTA were both present in the solution of silver (I) ions, in the ratio 2.5:1.00 (same ratio of NH_3 and HEDTA that was used in the potentiometric titration of S_3 solution), a change was observed in the silver deposition potential and current density (Fig. 2, dashed- pointed curve (- • -)), in comparison with the voltammetric curves obtained with solutions containing only NH_3 or HEDTA. This result indicated that in this solution, the silver(I) ions were reduced from a mixture of $[AgHEDTA]^{2-}$ and $[Ag(NH_3)_2]^+$.

Figure 2(b) shows voltammetric curves for silver electrodeposition on a platinum substrate from ammonium-buffered solutions containing various HEDTA concentrations. It can be observed that the current density and the potential of silver deposition with 2.0×10^{-3} M and 2.0×10^{-2} M HEDTA were not significantly different from the values without additive, indicating that silver was reduced from the same ion complex, i. e., $[Ag(NH_3)_2]^+$. The small shift in the deposition potential may be attributed to the HEDTA anion adsorption on the Pt substrate. Conversely, with 2.0×10^{-1} M HEDTA (solid curve) in the plating bath, the silver deposition potential was changed by about 100 mV in direction to more negative values, and the deposition current density is significantly decreased twofold in the region from –0.100 V down to –0.700 V. As mentioned above, this occurred due to the silver reduction from a mixture of $[AgHEDTA]^{2-}$ and $[Ag(NH_3)_2]^+$.

Silver electrodeposition on to a Pt rotating disk electrode (RDE) was studied in ammonium-buffered plating baths with 2.0×10^{-2} M, 2.0×10^{-1} M HEDTA and without HEDTA, in order to confirm that the silver deposition process was controlled by mass transport and that the decrease in current density occurred because of a change in the electroactive species. Figure 3 shows the plots of i^{-1} versus $f^{-1/2}$ for these solutions, which verified that the deposition process was controlled by mass transport. The diffusion coefficients (*D*) for silver complexes in the plating baths without and with HEDTA were estimated based on a kinematic viscosity of 0.01 cm^2 s^{-1}. The value of *D* in

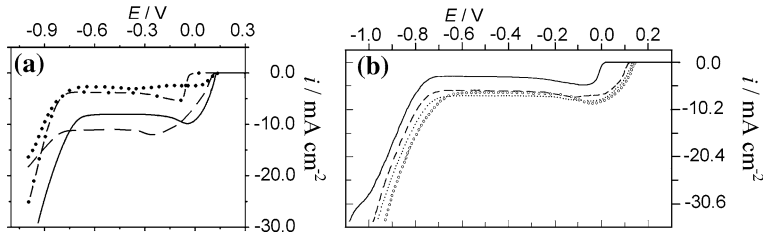

Fig. 2 Voltammetric curves for silver deposition on a platinum substrate from: (**a**) (——) 1.0×10^{-1} M $AgNO_3$ + 5.0×10^{-1} M NH_3 + 1.0×10^{-1} M NH_4NO_3, (– – –) 1.0×10^{-1} M $AgNO_3$ + 6.0×10^{-1} M NH_3, (• • •) 1.0×10^{-1} M $AgNO_3$ + 2.0×10^{-1} M HEDTA and (- • -) 1.0×10^{-1} M $AgNO_3$ + 2.0×10^{-1} M HEDTA + 5.0×10^{-1} M NH_3 + 1.0×10^{-1} M NH_4NO_3; (**b**) 1.0×10^{-1} M $AgNO_3$ + 5.0×10^{-1} M NH_3 + 1.0×10^{-1} M NH_4NO_3 with: (——) 2.0×10^{-1} M HEDTA, (– – –) 2.0×10^{-2} M HEDTA, (• • •) 2.0×10^{-3} M HEDTA and (○ ○ ○) without additive. υ = 10.0 mV s^{-1}. Potential values were referred to the Hg/HgO, 1.0 M NaOH electrode

the absence of HEDTA (1.86×10^{-5} cm^2 s^{-1}) and in the presence of 2.0×10^{-2} M HEDTA (1.87×10^{-5} cm^2 s^{-1}) in the plating bath are very similar, whereas that for 2.0×10^{-1} M HEDTA is significantly smaller (0.55×10^{-5} cm^2 s^{-1}). This result corroborates the hypothesis, based on the data in Fig. 2(b), that at a low HEDTA anion concentration ($\leq 2.0 \times 10^{-2}$ M) the silver is deposited from the diamminesilver(I) complex, whereas at a high HEDTA anion concentration ($\geq 2.0 \times 10^{-1}$ M) the deposition probably occurs from a mixture of complexes.

Considering that in ammonium-buffered solution containing at 2.0×10^{-1} M HEDTA, silver (I) ions are complexed with HEDTA and NH_3 further electrochemical studies were carried out for silver electrodeposition on the Pt substrate. To explain the deposition voltammogram (Fig. 4(a)) more clearly, it has been divided into four regions: I, II, III, and IV. In region I the increase in the cathodic current density is due to a rising rate of reduction of the silver (I) complex with rising polarity, while region II is characterized by a diffusion-limited current density. Beyond this region, the current density increases again, due to the hydrogen evolution reaction (HER), which occurs in parallel with silver deposition (region III). Finally, beyond ~–1.100 V (region IV), the current density increases further, due to the significant hydrogen evolution. In the anodic branch, two regions labeled a_1 and a_2 can be seen. The region a_1 was attributed to the formation of silver oxide, which at the peak fell from the electrode surface, leading to decrease in the current density and formation of the peak in the region a_1. After this, the current density increased a little (region a_2) until the silver film had gone from the electrode surface, leading to a decrease in the current density to zero. Han et al. [28] report a Pourbaix diagram (Eh – pH) for silver in ammonia solution. This Pourbaix diagram indicates that at pH greater than about 6, silver can form either diaminesilver(I) complex or oxide, depending on the potential and pH.

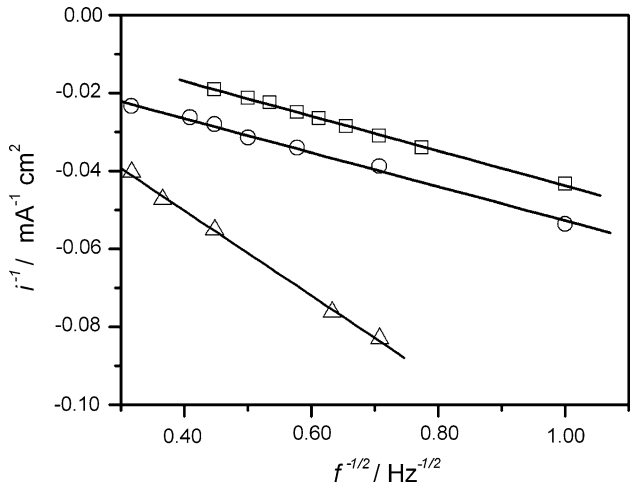

Fig. 3 Plot of i^{-1} versus $f^{-1/2}$ obtained from voltammetric curves for a rotating platinum substrate in 1.0×10^{-1} M M $AgNO_3$ + 5.0×10^{-1} M M NH_3 + 1.0×10^{-1} M M NH_4NO_3, with various HEDTA concentrations: (Δ Δ Δ) 2.0×10^{-1} M HEDTA, (○ ○ ○) 2.0×10^{-2} M HEDTA and (□ □ □) without additive. υ = 2.0 mV s^{-1}

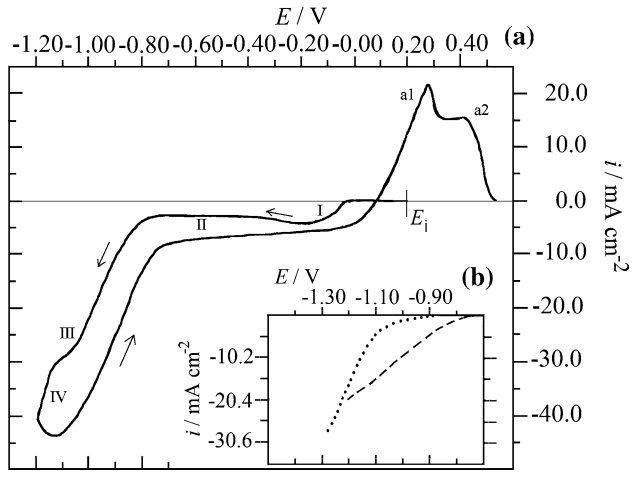

Fig. 4 (a) Voltammetric curve for a platinum substrate in 1.0×10^{-1} M $AgNO_3$ + 2.0×10^{-1} M HEDTA + 5.0×10^{-1} M NH_3 + 1.0×10^{-1} M NH_4NO_3; (b) Voltammetric curves for (– – –) platinum and (• • •) silver substrates in 2.0×10^{-1} M HEDTA + 5.0×10^{-1} M NH_3 + 1.0×10^{-1} M NH_4NO_3. υ = 10 mV s^{-1}. Potential values were referred to the Hg/HgO, 1.0 M NaOH electrode

Thus, the dissolution of silver film in the regions a_1 and a_2 occurred probably as described in Eqs. 2, 3, and 4:

$$Ag + 2NH_3 + H_2O \rightarrow Ag_2O_{(s)} + 2NH_4^+ + e^- \quad (2)$$

$$Ag_2O_{(s)} + 4NH_{3(aq)} + H_2O \rightleftharpoons 2[Ag(NH_3)]2^+ + 2OH^- \quad (3)$$

$$Ag_2O_{(s)} + HEDTA^{3-}_{(aq)} + H_2O \rightleftharpoons Ag(HEDTA)^{2-} + 2OH^- \quad (4)$$

Figure 4(b) shows typical cathodic voltammograms for platinum and silver electrodes in electrolytic solutions without silver ions. It can be seen that the HER, on platinum and silver, begins at –0.800 and –0.900 V, respectively. These results imply that HER is not a significant side reaction during the initial moments of the silver-plating process. Indeed, it is only significant beyond region II.

Sweep-reversal experiments were carried out in the early stages of silver deposition in a plating bath with 2.0×10^{-1} M HEDTA. Voltammetric curves with the sweep reversed at several different cathodic limit potentials are shown in Fig. 5. At a final potential of 0.000 V, the cathodic current in the reverse scan was greater, suggesting that the silver deposition occurred by nucleation [29, 30]. On the other hand, at limit potentials of –0.100 and –0.300 V, the current falls as the scan is reversed and a crossover is observed, showing that the silver deposition process is controlled by mass transport and occurs by nucleation, respectively.

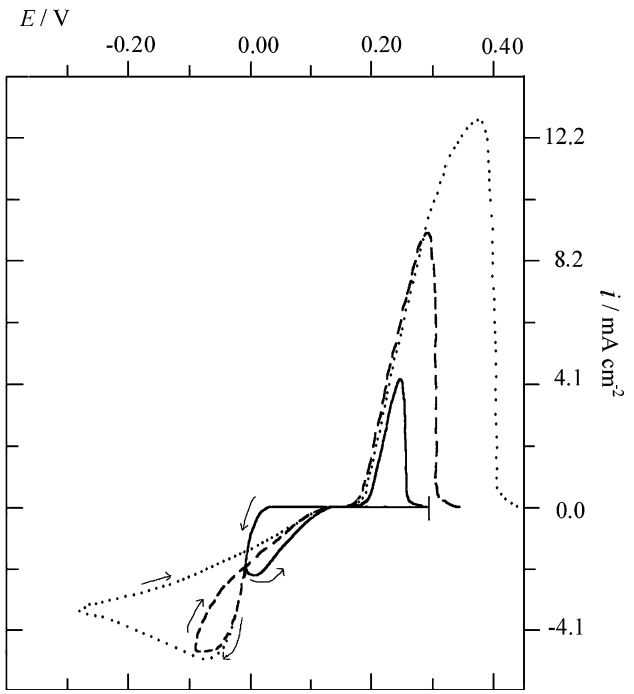

Fig. 5 Voltammetric curves for a platinum substrate in 1.0×10^{-1} M $AgNO_3$ + 2.0×10^{-1} M HEDTA + 5.0×10^{-1} M NH_3 + 1.0×10^{-1} M NH_4NO_3, showing effect of limit potentials: (——) 0.000 V, (– – –) –0.100 V and (• • •) –0.300 V. Potential values were referred to the Hg/HgO, 1.0 M NaOH electrode

A set of silver deposition voltammograms at various sweep rates (v) was recorded in the silver bath with 2.0×10^{-1} M HEDTA (Fig. 6(a)). Figure 6(a′) shows the influence of v in the region I of the voltammetric curve better. In Figs. 6 (b) and (c) the peak current density (i_p) from Fig. 6(a) is plotted against the square root of sweep rate ($v^{1/2}$) and the peak potential (E_p) versus v, respectively. These two graphs refer only to data from region I in Fig. 6(a), since in region III the HER occurs simultaneously with silver deposition. It can be seen in Fig. 6(b) that i_p increased non-linearly with $v^{1/2}$. Moreover, the peak potential (E_p) shifted negatively with increasing v (Fig. 6(c)). These results suggest that the silver electrodeposition process is quasi-reversible in this region [15, 22, 23].

Chronoamperometric study

Chronoamperometric study of silver electrodeposition from ammonium-buffered solution with 2.0×10^{-1} M HEDTA was carried out by step from 0.30 V to various potentials, corresponding to the beginning of the voltammetric curve (typical current transients in Fig. 7(a)), and at –0.200 V (Fig. 7(b)). This plating bath was chosen since it contains two silver complexes, which led to significant variation in the deposition voltammetric curve. At low overpotential (0.000 V to –0.050 V) the current transient curve showed two regions (I and II) of current density increases (typical transient was inserted in Fig. 7(a)) which correspond to different nucleation and growth processes. However, at –0.200 V (Fig. 7(b)) only one process was observed.

The current transients were analyzed by the equations of Scharifker and Hills [30] for 3D instantaneous and progressive nucleation controlled by mass transport. According to these authors, the instantaneous nucleation is given by:

$$I = \frac{zF\pi(2Dc)^{3/2}M^{1/2}t^{1/2}}{\rho^{1/2}} \quad (5)$$

and the progressive nucleation by:

$$I = \frac{zF\pi(2Dc)^{3/2}M^{1/2}Nt^{3/2}}{\rho^{1/2}} \quad (6)$$

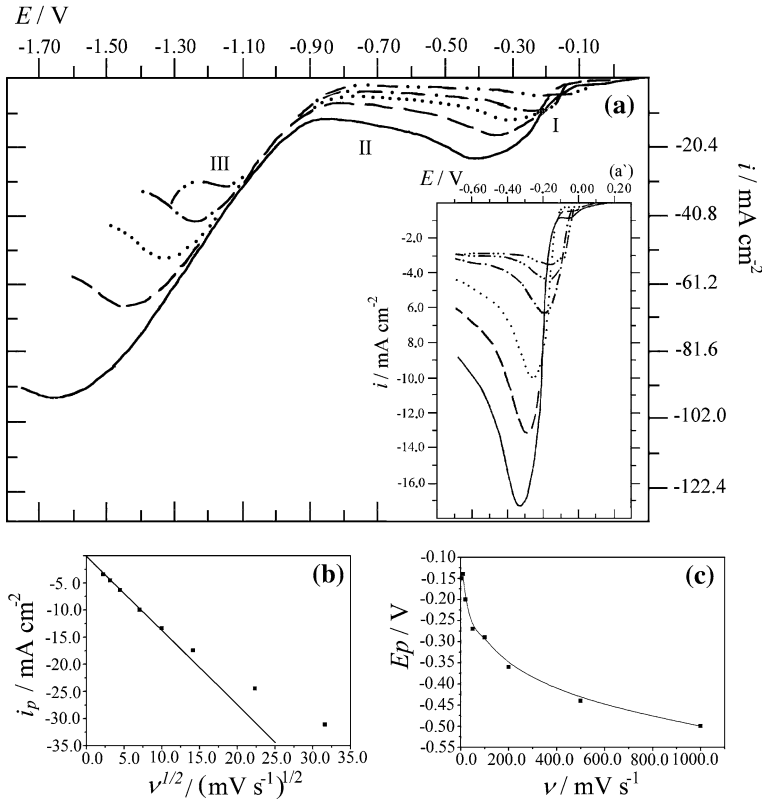

Fig. 6 (**a**) Voltammetric curves for a platinum substrate in 1.0×10^{-1} M $AgNO_3$ + 2.0×10^{-1} M HEDTA + 5.0×10^{-1} M NH_3 + 1.0×10^{-1} M NH_4NO_3, at various sweep rates (υ/mV s^{-1}): (**a**) (——) 500.0; (– – –) 200.0; (• • •) 100.0; (– • – •) 50.0, and (– • • –) 20.0. (**a′**) (——) 200.0, (– – –) 100.0, (• • •) 50.0, (– • – •) 20.0, (– • • –) 10.0, and (– • • •) 5.0; (**b**) Variation of i_p with $\upsilon^{1/2}$ and (**c**) variation of E_p with υ. Potential values were referred to the Hg/HgO, 1.0 M NaOH electrode

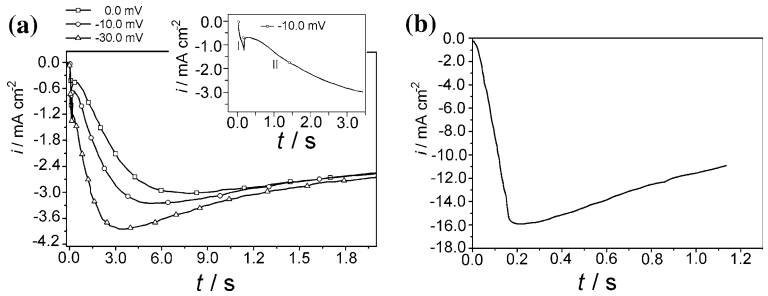

Fig. 7 Chronoamperometric curves for a platinum substrate in 1.0×10^{-1} M $AgNO_3$ + 2.0×10^{-1} M HEDTA + 5.0×10^{-1} M NH_3 + 1.0×10^{-1} M NH_4NO_3, obtained with step from 0.300 V to: (**a**) initial region of voltammetric deposition potential and (**b**) –0.200 V. Potential values were referred to the Hg/HgO, 1.0 M NaOH electrode

where D is the diffusion coefficient, c the bulk concentration, zF the molar charge on the electrodepositing species, M the molecular weight, ρ the density of the deposited metal and N the number of nuclei.

The analyses of regions I (Fig. 8(a, b)) and II (Fig. 8(c, d)) were carried out by plotting i versus $t^{1/2}$ and i versus $t^{3/2}$. The reasonable linearity of the curves showed in 8(b) and 8(c) suggests that at low overpotential, the nucleation changes form progressive (in region I) to instantaneous (in region II), during the same current transient.

Moreover, the current transient obtained by step from 0.30 V to –0.200 V was also analyzed by the dimensionless plot [31] for instantaneous nucleation, which is given by:

$$\frac{I^2}{I_m^2} = \frac{1.9542}{\left(t/t_m\right)}\left\{1 - \exp\left[-1.2564\left(\frac{t}{t_m}\right)\right]\right\}^2 \tag{7}$$

and for progressive nucleation by:

$$\frac{I^2}{I_m^2} = \frac{1.2254}{\left(t/t_m\right)}\left\{1 - \exp\left[-2.3367\left(\frac{t}{t_m}\right)^2\right]\right\}^2 \tag{8}$$

since at this potential the curve showed only one process.

The current transient obtained by step from 0.30 V to –0.200 V was analyzed by plotting (i/i_{max}) versus (t/t_{max}) and i verus $t^{3/2}$ (Fig. 9(a, b)). The results indicated 3D progressive nucleation controlled by mass transport.

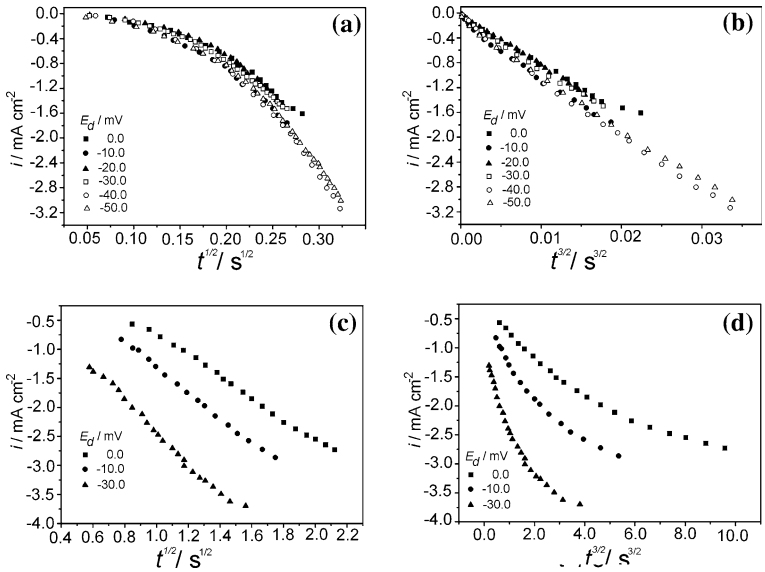

Fig. 8 Plots of i versus $t^{1/2}$ and i versus $t^{3/2}$ for current transient obtained with a step of potential to the beginning of the voltammetric deposition: (**a**, **b**) region I and (**c**, **d**) region II of the current transient shown in Fig. 7(a). Potential values were referred to the Hg/HgO, 1.0 M NaOH electrode

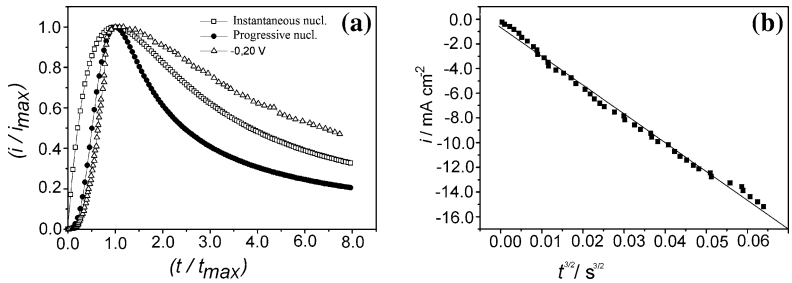

Fig. 9 Plots of (**a**) (i/i_{max}) versus (t/t_{max}) and (**b**) i verus $t^{3/2}$ for current transient obtained at –0.200 V versus Hg/HgO, 1.0 M NaOH electrode

These results showed that the nucleation was three-dimensional and corroborated the potentiodynamic studies with varying sweep-reverse potential, which indicated silver deposition by nucleation.

Analysis of the silver films by scanning electron microscopy

The morphology of the silver films was studied by scanning electron microscopy (SEM), in order to discover whether it was affected by the HEDTA anion concentration in the plating bath. The deposition potential was –0.200 V (region of diffusional control in the deposition voltammetric curve, Fig. 2(b)). In general, deposition on diffusional control leads to films of poor morphological quality. Then, the influence of additive was verified in this condition.

Figure 10(a–d) shows SEM micrographs of silver films deposited on Pt substrates from the plating bath, in the absence and presence of various HEDTA concentrations. Small globular crystallites and larger clusters of silver were obtained in the absence of HEDTA (Fig. 10(a)) in the plating bath. In contrast, when HEDTA was present, coalesced silver crystallites were obtained, regardless of its concentration (Figs. 10(b–d)). Comparing Fig. 10(a) and Fig. 10(b–d), it can be seen that HEDTA has brightening properties and improves the quality of the silver film.

These results are very significant for practical applications, since silver film morphology was not affected significantly by variations in the HEDTA anion concentration, from 2.0×10^{-3} M to 2.0×10^{-1} M, in the plating bath.

Moreover, the SEM results corroborated the chronoamperometric studies from solution containing 2.0×10^{-1} M HEDTA at –0.200 V, which indicated progressive nucleation, resulting in a film of crystallites with different size.

X-ray diffraction analysis of the silver films

X-ray diffraction analyses were carried out to establish the influence of the deposition potential and HEDTA concentrations on the silver film structure. The observed crystallographic distances, *d(hkl)*, were compared with the expected distance values given in JCPDS [32].

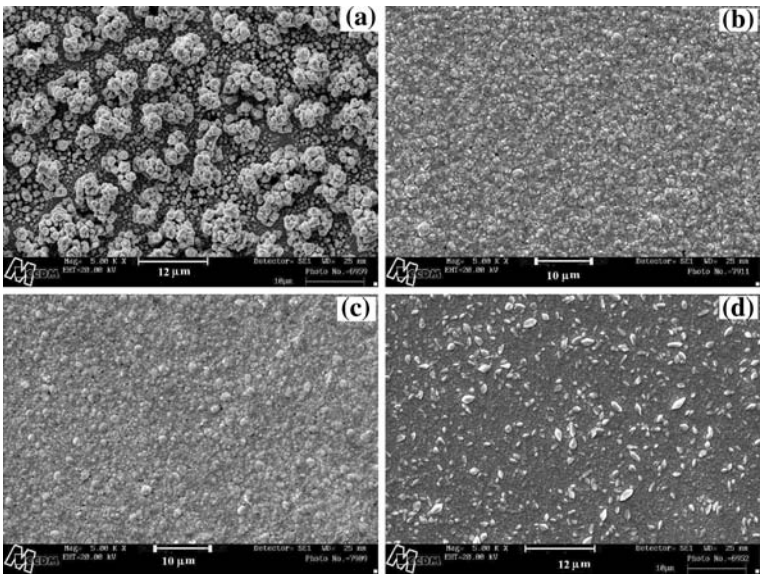

Fig. 10 SEM micrographs of silver deposited on platinum substrate a potential of –0.200 V (referred to the Hg/HgO, 1.0 M NaOH electrode) and q_d = 2.0 C cm^{-2} from 1.0×10^{-1} M $AgNO_3$ + 5.0×10^{-1} M NH_3 + 1.0×10^{-1} M NH_4NO_3 at various HEDTA concentrations: (**a**) in the absence of HEDTA, (**b**) 2.0×10^{-3} M, (**c**) 2.0×10^{-2} M, and (**d**) 2.0×10^{-1} M

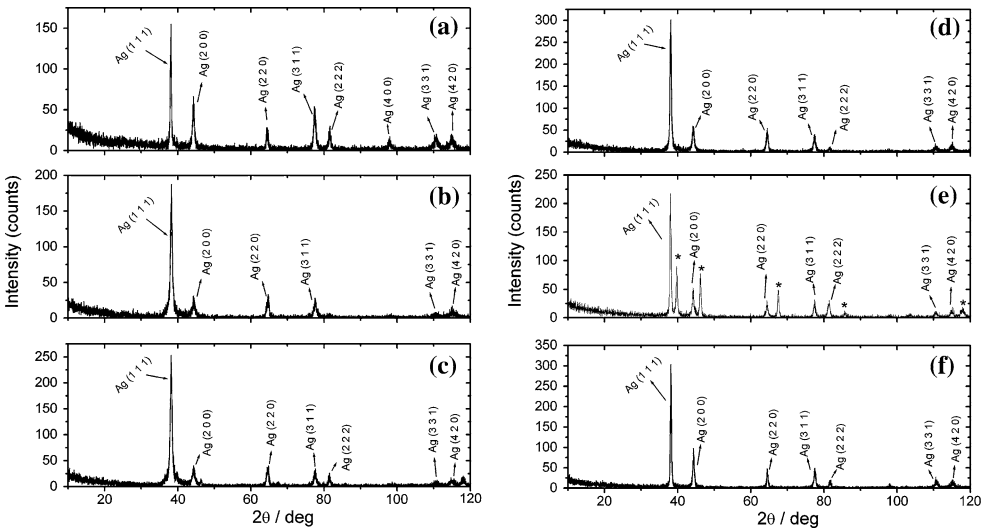

Fig. 11 Diffractograms of silver electrodeposited on platinum substrate at potential of –0.200 V (referred to the Hg/HgO, 1.0 M NaOH electrode) and q_d = 2.0 C cm^{-2}, from 1.0×10^{-1} M $AgNO_3$ + 5.0×10^{-1} M NH_3 + 1.0×10^{-1} M NH_4NO_3 at various HEDTA concentration: (**a**) in the absence of HEDTA, (**b**) 2.0×10^{-3} M, (**c**) 2.0×10^{-2} M, and (**d**) 2.0×10^{-1} M, and at potentials of (**e**) –1.100 V and (**f**) –0.050 V, with 2.0×10^{-1} M HEDTA in the plating bath. * platinum peaks

Figure 11 shows typical X-ray diffraction patterns of silver films deposited on platinum substrate by step from 0.30 V to –0.20 V from a solution with various HEDTA concentrations (Fig. 11(a–d) and from solution containing 2.0×10^{-1} M HEDTA at various deposition potential (Fig. 11(d–f)). These diffractograms showed similar patterns, indicating the occurrence of polycrystalline silver with the following reflections: (1 1 1), (2 0 0), (2 2 0), (3 1 1), (2 2 2), (3 3 1), and (4 2 0). Then, it could be concluded that neither the potential of deposition (Fig. 11(a), (e), and (f)) nor the HEDTA concentrations (Fig. 11(b–d)) led to changes in the silver structure. Moreover, the crystallographic structures of silver film obtained from solution containing different composition were similar, although its morphologies were different.

Conclusions

Potentiometric titrations and voltammetric studies showed that the HEDTA in the bath affected the silver electrodeposition process at high concentrations, when the silver reduction process occurred *via* a mixture of $[Ag(NH_3)]^+$ and $[Ag(HEDTA)]^{2-}$ complexes. The silver electrodeposition process is limited by mass transport and in solution containing 2.0×10^{-1} M HEDTA the diffusion coefficient of the mixture of silver(I) complexes was 5.5×10^{-6} cm^2 s^{-1}. Chronoamperometric study in solution containing 2.0×10^{-1} M HEDTA at low overpotential showed a progressive-instantaneous transition within a single transient, whereas at –0.200 V only 3*D* progressive nucleation controlled by mass transport was observed.

From the SEM micrographs, it could be inferred that HEDTA acted as a brightener. Silver films were adherent, uniform with fine granularity and fully covered the substrate. X-ray diffraction analysis of the silver films obtained from solutions containing various HEDTA concentrations indicated the occurrence of polycrystalline silver.

Acknowledgements Financial support from Brazilian agencies FAPESP (Proc. no. 02/10772-6 and 04/06413-6) and CAPES is gratefully acknowledged.

References

1. Bochkarev VA, Napukh ÉZ (1982) Soviet Electrochem 18:752
2. Gunawardena G, Hills G, Montegro I (1982) J Electroanal Chem 138:241
3. Papanastasiou G, Jannakoudakis D, Amblard J, Froment M (1985) J Appl Electrochem 15:71
4. Kristev I, Nikolova M (1986) J Appl Electrochem 16:703
5. Krishnan RM, Sriveeraraghavan S, Natarajan SR (1986) Bullet Electrochem 2(3):257
6. Michailova E, Milchev A (1991) J Appl Electrochem 21:170
7. Palomar-Pardavé M, Ramírez MT, González I, Serruya A, Scharifker BR (1996) J Electrochem Soc 143(5):1551
8. Miranda-Hernández M, González I (1997) Electrochim Acta 42(150):2295
9. Miranda-Hernández M, Palomar-Pardavé M, Batina N, González I (1998) J Electroanal Chem 443:81
10. Miranda-Hernández M, Palomar-Pardavé M, Batina N, González I (1998) Surf Sci 399:80
11. Reents B, Plieth W, Macagno VA, Lacconi GI (1998) J Electroanal Chem 453:121
12. Azzaroni O, Schilardi PL, Salvarezza RC, Arvia AJ (1999) Langmuir 15:1508
13. Fourcade F, Tzedakis T (2000) J Electroanal Chem 493:20
14. Krastev I, Zielonka A, Nakabayashi S, Inokuma K (2001) J Appl Electrochem 31:1041
15. de Oliveira GM, Barbosa LL, Broggi RL, Carlos IA (2005) J Electroanal Chem 578:151
16. Zarkadas GM, Stergiou A, Papanastasiou G (2005) Electrochim Acta 50:5022
17. Tulio PC (1996) Ph.D. Thesis, Universidade Federal de São Carlos, Brasil
18. Goldstein JI, Roming AD Jr, Newbury DE, Lyman CE, Echlin P, Fiori C, Joy DC, Lifshin E (1992) Scanning electron microscopy and X-ray microanlysis: a text for biologists, materials scientists, and geologists, 2nd edn. Plenum Press, New York
19. Carlos IA, Carlos RM, Caruso CS (1997) J Power Sources 69:37
20. Carlos IA, Souza CAC, Pallone EMJA, Francisco RHP, Cardoso V, Lima-Neto BS (2000) J Appl Electrochem 30:987
21. Carlos IA, Malaquias MA, Oizumi MM, Matsuo TT (2001) J Power Sources 92:56
22. de Almeida MRH, Carlos IA, Barbosa LL, Carlos RM, Lima-Neto BS, Pallone EMJA (2002) J Appl Electrochem 32:763
23. Carlos IA, Siquiera JLP, Finazzi GA, Almeida MRH (2003) J Power Sources 117:179
24. Carlos IA, de Almeida MRH (2004) J Electroanal Chem 562:153
25. Broggi RL, de Oliveira GM, Barbosa LL, Pallone EMJA, Carlos IA (2006) J Appl Electrochem 36:403
26. Cullity BD, Stock SR (2001) Elements of X-ray diffraction. Prentice-Hall, Inc., London
27. Kotrlý A, Šůcha L (1985) Handbook of chemical equilibria in analytical chemistry. John Wiley & Sons, New York
28. Starovoytov ON, Kim NS, Han KN (2007) Hydrometallurgy 86:114
29. Fletcher S (1983) Electrochim Acta 28(70):971
30. Fletcher S, Halliday CS, Gates D, Westcott M, Lwin T, Nelson G (1983) J Electroanal Chem 159:267
31. Scharifker BR, Hills G (1983) Electrochim Acta 28(7):879
32. Joint Committee on Powder Diffraction Standards (JCPDS), In: International Centre for Diffraction Data. Powder Diffraction File PDF-2. Database Set 1–49. Pennsylvania, ICDD, (2000) CD-ROM